Proceedings of the ASME 2025
International Design Engineering Technical Conferences and
Computers and Information in Engineering Conference
IDETC-CIE2025
August 17-20, 2025, Anaheim, CA

DETC2025-168610

COMPARING CUSTOM CNN AND TRANSFER LEARNING FOR DETAILED POWER LINE INSPECTION WITH A MOBILE DAMPING ROBOT

Ranhee Yoon, Hyun Myung Kang, Oumar Barry*
Department of Mechanical Engineering
Virginia Polytechnic Institute and State University
Blacksburg, Virginia 24061

ABSTRACT

The reliability of power line conductors is essential for safety and economic stability. Environmental factors—such as dust, moisture, and wind-induced vibrations—accelerate degradation, leading to reduced mechanical strength, increased electrical resistivity, and corrosion. To prevent unexpected failures, timely and systematic inspection is crucial. In this paper, we propose an autonomous inspection and classification framework for power line conductors. We define four conductor health conditions: Healthy, Minor Corrosion, Pollution-Induced Corrosion, and Pollution-Induced Fretting. Using a modified Mobile Damping Robot, we collected real-world images of both healthy and aged power lines on a testing structure. These images were subsequently processed with segmentation models like U-Net and the Segment Anything Model (SAM) to isolate the conductor against the background, optimizing the dataset for analysis. We explore two deep-learning approaches to classify the power line conditions. The first is a custom-designed Convolutional Neural Network (CNN), while the second utilizes transfer learning with ResNet-50 as the backbone. Both models were trained to distinguish the four conditions based on visual features, with performance validated on a dedicated testing set. The results demonstrate that the proposed models effectively classify power line conductor conditions. This approach offers a promising method for proactive conductor maintenance and enhances long-term grid reliability.

Keywords: Power Line, Health Monitoring, Transfer Learning, Image Segmentation, Classification, CNN, Robotics

*Corresponding Author (Email: obarry@vt.edu)

1 INTRODUCTION

The reliability of electric power infrastructure is critical to modern society, as failures in power lines can lead to severe economic and social consequences, including costly outages and safety risks. In the United States, power outages result in annual economic losses ranging from $25 billion to $70 billion [1–3]. Aging power line conductors, subjected to environmental and operational stresses, are particularly vulnerable to degradation, leading to reduced mechanical strength, increased electrical resistivity, and corrosion. Studies indicate that nearly half of controllable conductor failures derive from material degradation, with corrosion and fatigue being the primary contributors [4, 5]. Naranpanawe et al. [6] reported that corrosion alone accounts for 30% of controllable conductor failures, while fatigue contributes 14%, as shown in Fig. 1. Additionally, Zhang et al. [7] found that 67% of overhead line failures occur on conductors, with 64% of these being mechanical failures. These statistics underscore the urgent need for early identification and proactive management of deteriorating conductors to prevent catastrophic failures and ensure power grid reliability.

Traditional time-based maintenance strategies are limited in their ability to account for varying stress factors, often leading to either premature interventions or overlooked faults [6, 8]. In contrast, condition-based maintenance enables timely interventions based on actual conductor health. However, existing research on advanced condition monitoring technologies for power line conductors remains insufficient.

Current inspection methods primarily rely on manual visual assessments, which are subjective, labor-intensive, and prone to hu-

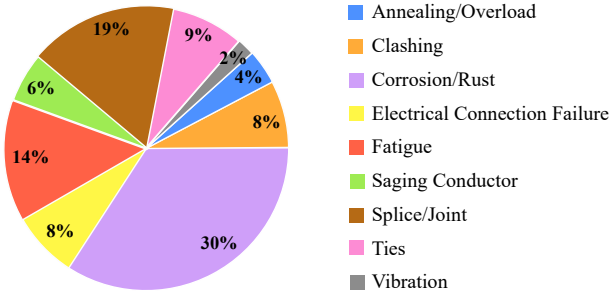

FIGURE 1: Different causes of conductor failure [6].

man error [9, 10]. Periodic inspections expose workers to safety hazards and fail to provide continuous monitoring. Aerial inspection methods, such as helicopters [11], satellites [12], or unmanned aerial vehicles (UAVs) [13], face operational constraints, including limited proximity to power lines, making detailed damage assessment challenging. While robotic systems [14, 15] such as LineScout [16], and Expliner [17] have demonstrated potential for automated inspection, they remain costly, bulky, complex, and require human intervention for operation. These challenges highlight the need for a fully autonomous, efficient, and cost-effective solution for accurate conductor health assessment.

Furthermore, existing assessment tools lack standardized guidelines for the detailed classification of damage types and severity levels. Advanced AI-driven image analysis is essential to enhance predictive maintenance by enabling early defect detection. The integration of autonomous robotic systems equipped with high-resolution imaging and AI-powered classification algorithms is crucial for improving conductor health assessment, reducing maintenance costs, and preventing unexpected failures.

This research introduces a novel robotic approach for power line conductor health monitoring, offering a new method for condition-based maintenance and establishing a foundation for future deployment in real-world environments. The proposed system consists of three key components: (1) Robot Design and System Architecture, where an autonomous robot is developed to collect conductor images and a testing fixture with an unique fixing mechanism ensures accurate image acquisition; (2) Image pre-processing, which employs U-Net and the Segment Anything Model (SAM) for background removal, followed by labeling images into four distinct classes: healthy, minor corrosion, pollution-induced corrosion, and pollution-induced fretting; and (3) deep learning-based classification framework, which compares transfer learning approaches (ResNet-50) and a custom design CNN based on performance metrics, computational efficiency, and training time. Lastly, with the testing dataset, we demonstrate the effectiveness of our model in improving reliability and efficiency in conductor assessment. This research introduces a novel robotic approach for power line conductor health monitoring, presenting a new method in predictive maintenance.

2 ROBOT DESIGN AND SYSTEM ARCHITECTURE

Most existing robotic inspection systems are complex, bulky, and not fully autonomous [14–17]. The Mobile Damping Robot (MDR) integrates power line health inspection with the damping properties of aeolian vibration dampers, as demonstrated in previous research [18]. By incorporating vibration control characteristics, the MDR eliminates the need for complex climbing mechanisms over dampers while enhancing vibration mitigation by positioning itself near the nearest anti-node and adapting to changing wind conditions [19–21]. The prototype design of the MDR is shown in Fig. 2.

FIGURE 2: Conceptual design model of the MDR [20].

This section details the development of the modified MDR framework, which was accomplished in two phases. In the first phase, the robot was modified to integrate essential components—microcontrollers, cameras, and power systems—while the design was refined to ensure a secure grip and smooth traversal along conductors. The second phase involved designing and constructing a test fixture equipped with a unique conductor-fixing mechanism, enabling the robot to attach securely to the conductor and capture high-quality images for analysis.

2.1 Robot Design

Modifications to the previous robot design were necessary to integrate essential sensors and enhance functionality. While retaining the basic structure and gripping mechanism, we incorporated additional components such as a camera, Raspberry Pi, motor controller, servo motor, battery, and Bluetooth module to enable health monitoring and inspection capabilities (Fig. 3). This design forms a meaningful basis for future adaptation to field conditions, even though further refinements are still needed.

Initially, the robot's outer shell was redesigned to incorporate flat surfaces, reducing complexity in both manufacturing and testing—particularly in the 3D printing process. Since we relied on basic-functionality 3D printers, simplifying the design was critical to ensuring consistent prints. PLA was selected as the printing material, and the flat surfaces also eased the attachment of electronic components.

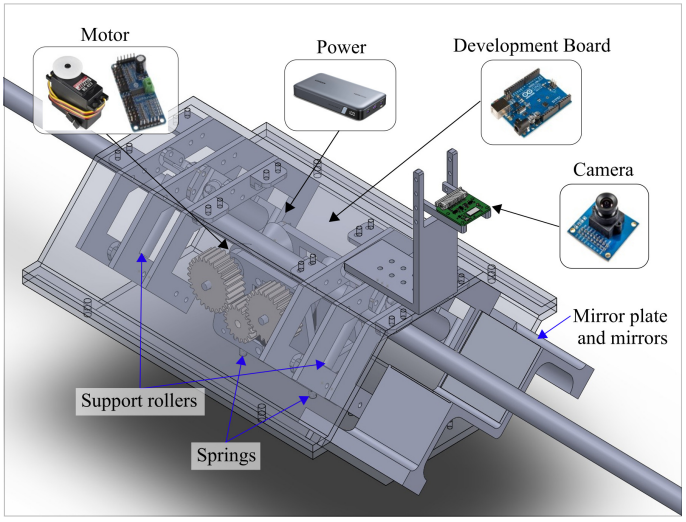

FIGURE 3: CAD design of the modified MDR.

Another key system integration enables the robot to capture images of the power line conductor from all angles, ensuring full visual coverage for effective inspection. To achieve this, we modified the previous senior design's mirror plate and integrated it into our MDR robot. Figure 3 illustrates our modified mirror plate design, where the mirror is angled 45° from the vertical centerline, optimizing the viewing angles for a complete image of the power line. The camera is positioned vertically to directly capture the conductor, while the mirror provides two additional reflected views, as shown in Fig. 6.

To ensure accurate classification through vision-based inspection, the camera requires relatively high resolution, as detailed images of the conductor provide valuable data for analysis. In parallel, the motor supports precise movements. These modifications enable the robot to efficiently capture and process high-quality images, supporting automated and reliable data collection for the health inspection system.

Furthermore, the robot incorporates an adaptable gripping mechanism to accommodate conductors of varying diameters. This mechanism features four support rollers arranged in a triangular configuration at the top, with the motor base mounted at the bottom of the case. Springs positioned between these components apply a constant yet flexible force, ensuring that the rollers maintain sufficient friction against the conductor while allowing the robot to adapt to different sizes. To maintain simplicity and focus on this study's primary objectives, we intentionally excluded the vibration damper from the design. Moreover, aspects such as structural rigidity, environmental protection, and outdoor simulation were deemed beyond the scope of this prototyping stage.

Figure 4 summarizes the robot's software logic. The system captures two types of images: one focused on the conductor and the other on its reflection. After saving these images, the Raspberry Pi communicates with the motor controller to move the servo motor by a specified distance. This process repeats for a predefined number of positions, as specified by the user.

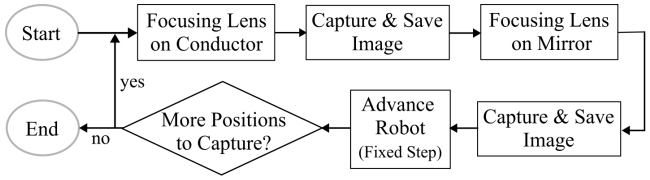

FIGURE 4: Image acquisition process with the MDR.

2.2 Laboratory Setup for Data Acquisition

A controlled laboratory setup was established to facilitate structured data acquisition for evaluating the autonomous mobile robot's ability to capture high-quality conductor images. This setup ensured precise image acquisition while minimizing potential interference and structural wear on the conductor.

As illustrated in Fig. 5, a testing fixture was designed to securely hold the power line conductor while reducing abrasion between the conductor and the wooden structure. A pulley mechanism was integrated into the design, enabling smooth sliding of the conductor along its length. This allowed the robot to traverse the conductor without obstruction, ensuring consistent image acquisition. Additionally, a friction-based clamping mechanism secured the conductor at its base, eliminating the need for traditional tensioning methods that require looping the conductor's ends. This design enhanced operational efficiency and maintained image integrity during testing.

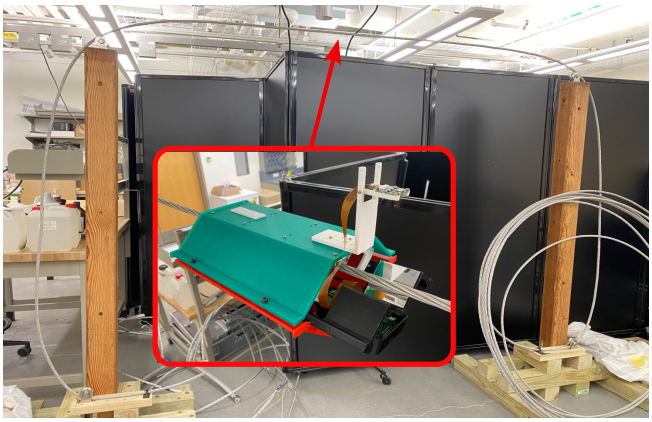

FIGURE 5: Testing fixture with the MDR mounted.

Two types of conductors were used: a new conductor that had been previously used for vibration experiments in the lab and a

worn-out conductor that was removed from service and retrieved from an electric service company. The worn-out conductor exhibited real-world degradation, including surface wear and corrosion, making it an essential reference for testing the system's capability to detect damage under practical conditions.

During data acquisition, the robot is mounted onto the conductor and moves along it in controlled increments, capturing images at each step. Once acquisition is complete, the images are transferred to a desktop computer, where computer vision and machine learning algorithms process them. The robot's movement is synchronized with the motor controller, ensuring precise positioning for consistent image capture. Figure 6 presents sample images obtained through this process. The system's effectiveness is evaluated using a dataset of approximately 5,000 images acquired with the prototype robot.

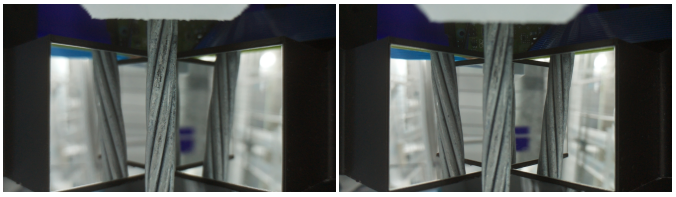

(a) (b)

FIGURE 6: Two images acquired by the MDR: (a) Lens focused on the conductor, (b) Lens focused on the mirror reflection

3 IMAGE PRE-PROCESSING

The image preprocessing method from previous research [22] did not include background removal, as conductor images were captured under controlled conditions with a plain white sheet as the background. However, in this study, background removal was incorporated since images captured by the robot contain surrounding objects that introduce noise. Without this step, the classification models' effectiveness would be impacted [23, 24]. The finalized background removal procedure, optimized for image analysis, is illustrated in Fig. 7.

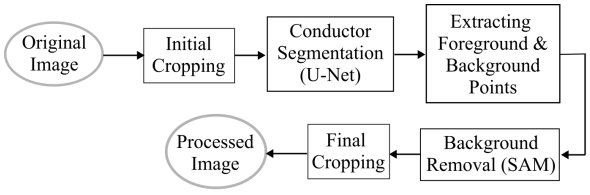

FIGURE 7: Background removal process.

Once the background is removed, the processed images are labeled for conductor health classification. Conductors are categorized based on surface conditions to ensure accurate assessment. Proper labeling enables the deep learning model to differentiate varying levels of degradation, improving classification reliability. By systematically organizing the dataset into meaningful health categories, the model is trained to detect and predict conductor conditions with greater precision and interpretability.

3.1 Background Removal Using U-Net and SAM

The testing fixture uses a friction-based clamping mechanism to secure and tension the conductor. However, this clamping method does not include a complete tensioning system, which results in slight bending at the contact points due to applied pressure. This bending affects the conductor's position and angle in the images. Accurate background removal requires proper selection of input and background points, but the variations in conductor position and angle make relying on predefined points unsuitable. To overcome this challenge, the U-Net segmentation model is used to precisely identify the conductor's position and angle in each image. U-Net [25], a fully convolutional neural network designed for image segmentation, features an encoder-decoder architecture that allows for accurate localization of objects. Its skip connections preserve spatial information, making it highly effective for segmenting conductors despite variations in positioning.

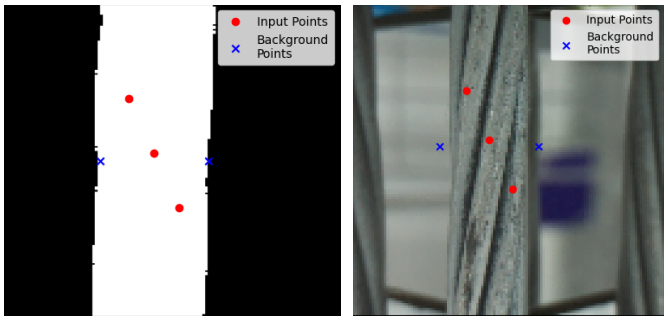

(a) (b)

FIGURE 8: Results of images processed with U-Net: (a) Segmented binary mask, (b) Original image.

As shown in Fig. 8, the conductor is segmented from the background using U-Net, generating a mask that guides the selection of input and background points. Background points are placed to the left and right of the segmented conductor at the mid-height of the image, with values slightly smaller than those in the segmentation mask. Input points are strategically positioned diagonally across the conductor to optimize line detection.

The binary mask derived from U-Net is used to automate the positioning of input and background points for background removal with SAM, developed by Meta AI [26]. In this study, we applied the *ViT-L* SAM model, which strikes the best balance between processing time and segmentation quality. Figure 9 illustrates

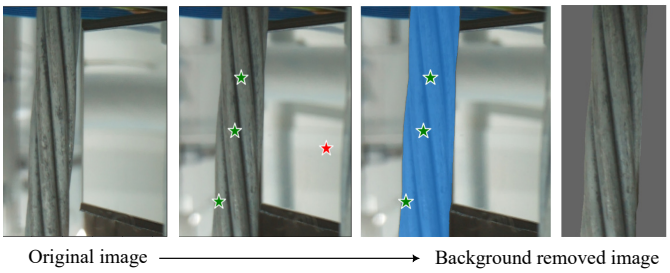

FIGURE 9: Result of background removal using SAM.

an example of this process, where SAM effectively removes the background by utilizing the segmentation mask generated by U-Net. This method ensures precise isolation of the conductor while eliminating surrounding noise. The entire background removal process takes less than 0.5 seconds per image, achieving an accuracy of around 90%. Future optimization of input and background points could further improve accuracy.

3.2 Conductor Health Labeling

The preprocessed images are shown in Fig. 10. Following the background removal process, the images were categorized into four distinct classes: Healthy, Minor Corrosion, Pollution-Induced Corrosion, and Pollution-Induced Fretting. The Healthy class consists of images captured from a new conductor used in vibration experiments in the lab, as it was free from any visible degradation. In contrast, the worn-out conductor exhibited gray discoloration and a loss of luster due to surface-wide corrosion, which, though not critically harmful to conductor health, is categorized as Minor Corrosion [27]. Thus, in total, we obtained the images with two conductors, healthy and worn out.

In some areas, the worn-out conductor showed black dust accumulation. When dust and foreign contaminants accumulate on the roughened, corrosion-infused surface, it increases the temperature of the conductor, even with the same amount of current, significantly affecting its performance and conditions [28]. Images of aged conductors with visible contamination and very minor abrasion are classified as Pollution-Induced Corrosion. Finally, the Pollution-Induced Fretting class includes images showing distinct signs of both major abrasion and pollution-induced corrosion, representing the most critical condition.

4 DEEP LEARNING-BASED CLASSIFICATION FRAMEWORK

To automate the classification of power line conductor images into four distinct categories, we implemented two neural network approaches: a custom CNN trained from scratch and a transfer learning model using ResNet-50 as the backbone. For both models, we employed the Adam optimizer with weight decay to mitigate overfitting and address dataset imbalance [29]. To enhance generalization, we incorporated image augmentation techniques during training [30]. Additionally, we used a learning rate scheduler that reduces the learning rate when training performance plateaus, thereby improving convergence [31]. Both approaches were optimized using multi-category cross-entropy loss, which has consistently demonstrated robust performance for multi-class classification tasks. The loss function is defined in the equation 1,

FIGURE 10: Final result of images with the background removed: (a) Healthy, (b) Minor corrosion, (c) Pollution-induced corrosion, (d) Pollution-induced fretting.

$$\mathscr{L}_{CE} = -\sum_{i=1}^{N}\sum_{c=1}^{C} y_{i,c}\log\left(\hat{y}_{i,c}\right), \tag{1}$$

where $y_{i,c}$ represents the one-hot encoded true label and $\hat{y}_{i,c}$ is the predicted probability for class c.

4.1 Custom Convolutional Neural Networks

The rise of Convolutional Neural Networks (CNNs) has transformed image analysis across numerous fields. In medicine, for example, CNNs have been successfully integrated to automate and enhance diagnostic processes. These networks are particularly effective in classifying complex imaging data, such as CT scans for detecting brain tumors [32], X-rays for identifying COVID-19 [33], and skin diseases [34].

CNNs consist of multiple layers that progressively extract and refine features from input images. The initial convolutional layers use learnable filters to detect low-level features such as edges and textures. As data advances through the network, higher-level layers capture increasingly abstract representations. Pooling layers reduce the spatial dimensions of these feature maps, decreas-

ing the computational load and providing invariance to minor translations. Finally, fully connected layers interpret these abstract features to produce the final predictions [33]. Training a CNN involves a feed-forward pass, where input data is propagated through each layer to produce an output, followed by backpropagation, during which the network's weights are updated based on the computed error. This iterative process, typically guided by optimization algorithms over many epochs, continues until convergence is achieved.

For our custom CNN architecture (see Fig.11), colored (RGB) images of size 128 × 128 are processed through four convolutional blocks. The first block begins with a 3 × 3 convolution that increases the input channel count from 3 to 32, and subsequent blocks further increase the feature map dimensions to 64, 128, and finally 256. In each block, batch normalization is applied to stabilize the distribution of layer inputs, thereby accelerating training. This is achieved by augmenting layers that set the mean and variance of each activation's distribution to zero and one [35]. The ReLU activation function, defined in the equation 2,

$$\sigma(x) = \max\{0, x\} \tag{2}$$

introduces the necessary non-linearity to enable the network to capture complex patterns [36]. Following these operations, a 2 × 2 max pooling layer reduces the spatial dimensions, and dropout is employed to mitigate overfitting. Notably, the first two blocks use a dropout rate of 0.3, while the third and fourth blocks use a rate of 0.4 to enhance generalization further.

After the convolutional blocks, the feature maps are flattened and passed to a fully connected classifier with three linear layers. The first two linear layers use ReLU activations and a dropout rate of 0.5, while the final layer outputs logits for four classes. This structured design enables the network to efficiently learn and generalize from the diverse features present in the dataset.

4.2 Transfer Learning

The limited generalization observed in the model is partially attributed to the restricted dataset for training, both in terms of total number and class imbalance. As previously mentioned, the MDR captured conductor images. However, due to resource constraints—including the limited availability of aged power line conductors, the time-intensive nature of the data collection, and operational limitations—the dataset comprises approximately 5,000 unique images spanning various classes. Ideally, a larger and more balanced dataset would enhance model performance. Nevertheless, given these constraints, transfer learning emerges as a highly effective strategy for training with a limited dataset.

Barman has highlighted several advantages of transfer learning over training from scratch. Specifically, transfer learning requires

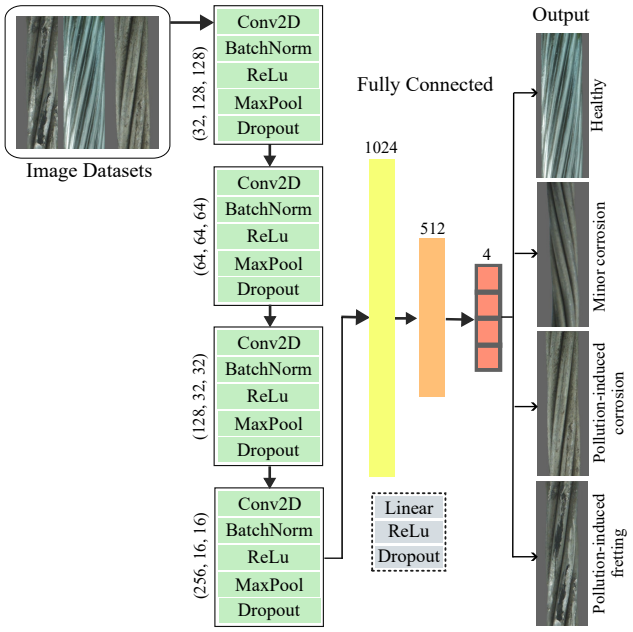

FIGURE 11: CNN model architecture.

fewer data samples to achieve similar performance, consumes less computational power, and accelerates model convergence. While it does have certain disadvantages, such as reduced flexibility in integrating new image datasets or adapting to unique data characteristics, it is ideally suited to our research objectives [37,38].

We selected ResNet-50 as the backbone for our image classification model due to its robustness and ability to address the vanishing gradient problem. While various pre-trained models (e.g., VGG, GoogLeNet, MobileNet, Xception) exist, ResNet-50's widespread use highlights its reliability. Deeper networks often suffer from diminishing gradients, hindering training [39], but ResNet-50 mitigates this with skip connections that preserve gradient flow, enabling deeper model training. Many object detection systems leverage ResNet variants (e.g., ResNet-50, ResNet-101, ResNet-152) for this reason [40]. Furthermore, ResNet-50 strikes an excellent balance between performance, computational cost, and ease of use when leveraging pre-trained weights in a transfer learning setup. Given the subtle differences in texture and severity among our images, ResNet-50 provides the necessary depth and feature extraction capabilities to effectively distinguish between the various classes.

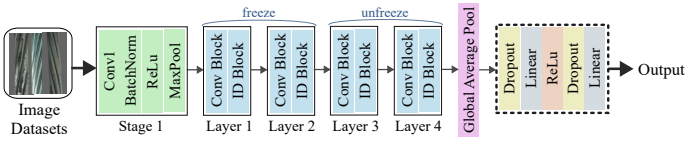

FIGURE 12: ResNet-50 model architecture.

Figure 12 illustrates the architecture of our model, which utilizes a pre-trained ResNet-50. In this design, we freeze the initial layers (layers 1 and 2) to retain the low-level features acquired during pretraining, while fine-tuning the deeper layers (layers 3 and 4). This selective approach is particularly advantageous when working with limited datasets; training all layers could lead to overfitting, whereas freezing all layers might hinder the network's ability to adapt to the new task [41]. By unfreezing only layers 3 and 4, the model can adjust higher-level, task-specific features without the excessive burden of updating all parameters.Following these adjusted layers, we replace the original fully connected (FC) layer with a custom classifier that includes an intermediate layer. This tailored classifier begins with a dropout layer set at a rate of 0.4 to mitigate overfitting. It then incorporates a linear layer that expands the feature dimensions to 512, followed by a ReLU activation function to introduce non-linearity. Another dropout layer precedes the final linear layer, which maps these features to the four output classes. This structured reduction—from a 512-dimensional feature space down to four class scores—facilitates smoother adaptation to the target domain.

5 EXPERIMENTS

Using the MDR, we assembled a dataset of 4,725 images across four conductor-health classes. We split these into an 80% training set (3,780 images) and a 20% test set (945 images). The training set exhibited severe class imbalance—Healthy: 1,004; Minor Corrosion: 387; Pollution-Induced Corrosion: 1,201; Pollution-Induced Fretting: 1,197 images—so we applied weight decay in our optimizer to help counteract bias during learning. To improve generalization, we also employed standard data-augmentation techniques: horizontal and vertical flips, rotations, random crops and translations, and brightness/contrast adjustments. Each augmentation operation was applied independently to every original training image, yielding one new variant per operation.

For both models, the initial learning rate was set to 0.0003, with the Adam optimizer used along with a weight decay of 0.0001 to manage the imbalanced dataset effectively. A learning rate scheduler with a factor of 0.1 and a patience count of three epochs was incorporated to reduce the learning rate when progress plateaued. Early stopping was applied with a patience of five epochs, halting training if the validation loss did not improve for five consecutive epochs, optimizing resource utilization. The model state corresponding to the lowest test error was saved after each epoch, ensuring that the best-performing weights were retained.

Training was conducted in a Google Colab environment, integrated with Google Drive for data storage. All evaluation and training processes were performed on an NVIDIA A100 GPU to ensure consistent performance metrics.

The training and test loss and accuracy plots are illustrated in Fig.13 and Fig.14. In our experiments, the custom CNN model completed training in 21 epochs, taking a total of 71.84 minutes. In contrast, the ResNet-50 model, utilizing transfer learning, required 32 epochs but completed training in 50.45 minutes. This suggests that, although ResNet-50 required more epochs, it achieved more efficient convergence per epoch, leading to a shorter overall training time compared to the custom CNN model. The final results are summarized in Table 1.

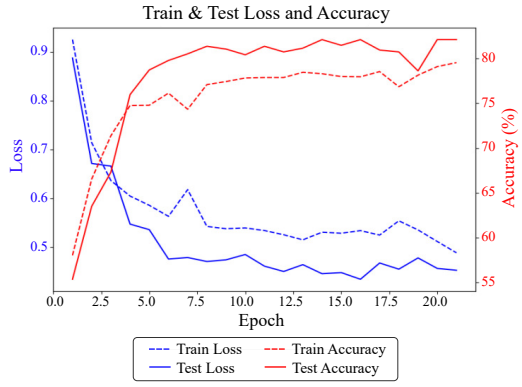

FIGURE 13: Loss and accuracy of training and test results with CNN model.

FIGURE 14: Loss and accuracy of training and test results with ResNet-50 model.

6 RESULTS AND DISCUSSION

The results, presented in Table 1, indicate that ResNet-50 outperforms the CNN model in all evaluated metrics. Not only does ResNet-50 require less training time, but it also consistently achieves superior performance. Specifically, ResNet-50 attained significantly lower training and test losses, with losses more than halved compared to the CNN. Regarding classification accuracy, ResNet-50 achieved 91.96% training accuracy and 91.53% test accuracy, while the CNN reached 79.55% training accuracy

TABLE 1: Results of experiments (CNN and ResNet-50 models).

	CNN	ResNet-50
Training Time [min]	72	50
Epoch [num]	21	32
Train Loss	0.49	0.20
Train Accuracy [%]	79.55	91.96
Test Loss	0.43	0.23
Test Accuracy [%]	82.12	91.53
Test Precision [%]	78.48	91.50
Test Recall [%]	82.12	91.53
Test F1 [%]	79.82	91.46

and 82.12% test accuracy. The close match between the training and test accuracies of ResNet-50 suggests that the model is well-designed and generalizes effectively. Furthermore, ResNet-50 exhibited higher precision (91.50%), recall (91.53%), and F1-score (91.46%), outperforming the CNN with respective values of 78.48%, 82.12%, and 79.82%. These findings highlight that ResNet-50 provides a more robust and accurate classification of conductor conditions.

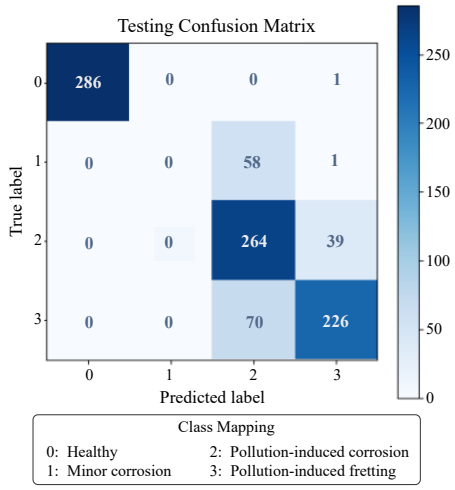

FIGURE 15: Confusion Matrix of CNN model test result.

The testing confusion matrices for the CNN and ResNet-50 models are presented in Fig.15 and Fig.16. The most notable improvement observed in ResNet-50 is its ability to classify the Minor corrosion class. While the CNN model failed to predict this class entirely, ResNet-50 correctly classified 39 out of 59 Minor corrosion images. Both models accurately classified the Healthy class with no misclassifications; however, they exhibited confusion among the remaining classes. This is likely because Healthy class images are distinctly different from those in the other classes.

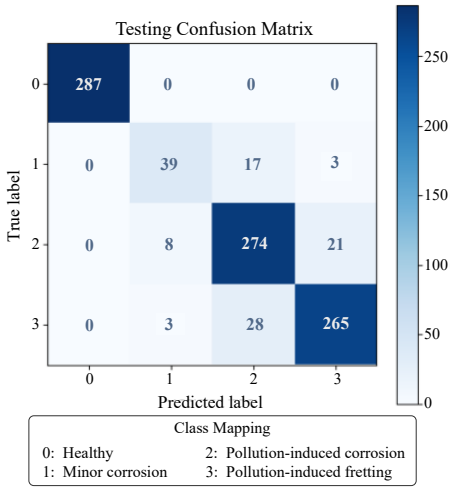

FIGURE 16: Confusion Matrix of ResNet-50 model test result.

ResNet-50 demonstrated classification errors of 34% for Minor corrosion, 14% for Pollution-induced corrosion, and 8% for Pollution-induced fretting. A primary reason for the high error rate in the Minor corrosion class could be the limited availability of training data. Additionally, misclassifications among the Minor corrosion, Pollution-induced corrosion, and Pollution-induced fretting classes suggest that certain images contain overlapping features, making accurate differentiation challenging. Addressing this issue will require further model improvements and potentially expanding the dataset.

Despite these challenges, ResNet-50 achieved an overall accuracy of about 92%, significantly outperforming the CNN model in classifying the three corrosion-related classes. These results highlight the potential of ResNet-50 for more accurate conductor condition classification.

7 CONCLUSION

In this paper, we present an autonomous inspection and classification framework for power line conductors. While the MDR is not yet ready for real-world deployment, we implemented deep learning models that achieved high accuracy in evaluating conductor health conditions. Among the models tested, ResNet-50 outperformed a custom CNN, underscoring its superior performance in classification tasks. Future work will explore the integration of the Consistent Rank Logits (CORAL) method to better capture the ordinal relationships among conductor condition categories. This study demonstrates the potential of advanced machine learning techniques to enhance the efficiency and reliability of power line maintenance.

ACKNOWLEDGMENTS

This work is funded by National Science Foundation CAREER Award ECCS 1944032: Towards a Self-Powered Autonomous Robot for Intelligent Power Lines Vibration Control and Monitoring. Any opinions, findings, and conclusions or recommendations expressed in this material are those of the author(s) and do not necessarily reflect the views of the National Science Foundation.

REFERENCES

[1] Michael J Sullivan. Estimated value of service reliability for electric utility customers in the united states. 2009.

[2] Oumar Barry, JW Zu, and DCD Oguamanam. Nonlinear dynamics of stockbridge dampers. *Journal of Dynamic Systems, Measurement, and Control*, 137(6):061017, 2015.

[3] Aman Ankit, Zhanlin Liu, Scott B Miles, and Youngjun Choe. Us resilience to large-scale power outages in 2002–2019. *Journal of safety science and resilience*, 3(2):128–135, 2022.

[4] Masoud Farzaneh and Konstantin Savadjiev. Evaluation of tensile strength of acsr conductors based on test data for individual strands. *IEEE Transactions on Power Delivery*, 22(1):627–633, 2007.

[5] Alan Rondineau, Laurent Gaillet, Lamine Dieng, and Sébastien Langlois. Degradation of steel wires in bimetallic aluminum–steel conductors exposed to severe corrosion conditions. *Corrosion and Materials Degradation*, 3(4):646–660, 2022.

[6] Lakshitha Naranpanawe, Hui Ma, and Tapan Saha. Overhead conductor condition monitoring: Milestone report 1. *The University of Queensland, Brisbane, Australia*, 2018.

[7] Xiang Zhang and Ernst Gockenbach. Component reliability modeling of distribution systems based on the evaluation of failure statistics. *IEEE Transactions on Dielectrics and Electrical Insulation*, 14(5):1183–1191, 2007.

[8] Tibin Joseph, Carlos E Ugalde-Loo, Jun Liang, and Paul F Coventry. Asset management strategies for power electronic converters in transmission networks: Application to hvdc and facts devices. *IEEE access*, 6:21084–21102, 2018.

[9] Ahmad Bala Alhassan, Xiaodong Zhang, Haiming Shen, and Haibo Xu. Power transmission line inspection robots: A review, trends and challenges for future research. *International Journal of Electrical Power & Energy Systems*, 118:105862, 2020.

[10] Nazmi Ekren, Zehra Karagöz, and Mustafa Şahin. A review of line suspended inspection robots for power transmission lines. *Journal of Electrical Engineering & Technology*, 19(4):2549–2583, 2024.

[11] Lizhong Zhang, Lijun Yan, Lixin Meng, Xiaoming Li, and Shanglin Huang. The application study of helicopter airborne photoelectric stabilized pod in the high voltage power line inspection. pages 232–235, 08 2012.

[12] Leena Matikainen, Matti Lehtomäki, Eero Ahokas, Juha Hyyppä, Mika Karjalainen, Anttoni Jaakkola, Antero Kukko, and Tero Heinonen. Remote sensing methods for power line corridor surveys. *ISPRS Journal of Photogrammetry and Remote Sensing*, 119:10–31, 2016.

[13] Husam A. Foudeh, Patrick Chi-Kwong Luk, and James F. Whidborne. An advanced unmanned aerial vehicle (uav) approach via learning-based control for overhead power line monitoring: A comprehensive review. *IEEE Access*, 9:130410–130433, 2021.

[14] Jaka Katrasnik, Franjo Pernus, and Bostjan Likar. A survey of mobile robots for distribution power line inspection. *IEEE Transactions on power delivery*, 25(1):485–493, 2009.

[15] Angelo Pagnano, Michael Höpf, and Roberto Teti. A roadmap for automated power line inspection. maintenance and repair. *Procedia Cirp*, 12:234–239, 2013.

[16] Nicolas Pouliot, Pierre-Luc Richard, and Serge Montambault. Linescout technology opens the way to robotic inspection and maintenance of high-voltage power lines. *IEEE Power and Energy Technology Systems Journal*, 2(1):1–11, 2015.

[17] Paulo Debenest, Michele Guarnieri, Kensuke Takita, Edwardo F Fukushima, Shigeo Hirose, Kiyoshi Tamura, Akihiro Kimura, Hiroshi Kubokawa, Narumi Iwama, and Fuminori Shiga. Expliner-robot for inspection of transmission lines. In *2008 IEEE International Conference on Robotics and Automation*, pages 3978–3984. IEEE, 2008.

[18] Oumar R. Barry, Emadeddin Y. Tanbour, Nitish K. Vaja, and Hesham Tanbour. Asymmetric aeolian vibration damper, April 17 2018. US Patent 9,948,081.

[19] Paul-Camille Kakou. *Towards A Mobile Damping Robot For Vibration Reduction of Power Lines*. PhD thesis, Virginia Tech, 2021.

[20] Paul Kakou, Mohammad Bukhari, Jiamin Wang, and Oumar Barry. On the vibration suppression of power lines using mobile damping robots. *Engineering Structures*, 239:112312, 2021.

[21] Andrew Choi and Oumar Barry. Testing and validation of a mobile damping robot for power lines. *International Design*

Engineering Technical Conferences and Computers and Information in Engineering Conference., 87400, 2023.

[22] Hyun Myung Kang, Ranhee Yoon, and Oumar Barry. A vision-based health inspection of power line conductors for the mobile damping robot. In *International Design Engineering Technical Conferences and Computers and Information in Engineering Conference*, volume 88353, page V02BT02A047. American Society of Mechanical Engineers, 2024.

[23] Xian Tao, Dapeng Zhang, Zihao Wang, Xilong Liu, Hongyan Zhang, and De Xu. Detection of power line insulator defects using aerial images analyzed with convolutional neural networks. *IEEE transactions on systems, man, and cybernetics: systems*, 50(4):1486–1498, 2018.

[24] Xinbo Huang, Yiqun Wu, Ye Zhang, and Huiying Zhang. A method of transmission conductor-loosened detect based on image sensors. *IEEE Transactions on Instrumentation and Measurement*, 69(11):8783–8796, 2020.

[25] Olaf Ronneberger, Philipp Fischer, and Thomas Brox. U-net: Convolutional networks for biomedical image segmentation. In *Medical image computing and computer-assisted intervention–MICCAI 2015: 18th international conference, Munich, Germany, October 5-9, 2015, proceedings, part III 18*, pages 234–241. Springer, 2015.

[26] Alexander Kirillov, Eric Mintun, Nikhila Ravi, Hanzi Mao, Chloe Rolland, Laura Gustafson, Tete Xiao, Spencer Whitehead, Alexander C. Berg, Wan-Yen Lo, Piotr Dollár, and Ross Girshick. Segment anything. *arXiv:2304.02643*, 2023.

[27] Aluminum Electrical Conductor Handbook. Aluminum electrical conductor handbook. *DC: The Aluminum Association*, 1982.

[28] MM Salama. Thermal performance of an overhead transmission line under the influence of dust accumulation. *Energy conversion and management*, 41(12):1323–1334, 2000.

[29] Iren Valova, Christopher Harris, Tony Mai, and Natacha Gueorguieva. Optimization of convolutional neural networks for imbalanced set classification. *Procedia Computer Science*, 176:660–669, 2020. Knowledge-Based and Intelligent Information Engineering Systems: Proceedings of the 24th International Conference KES2020.

[30] Luke Taylor and Geoff Nitschke. Improving deep learning with generic data augmentation. In *2018 IEEE Symposium Series on Computational Intelligence (SSCI)*, pages 1542–1547, 2018.

[31] Ayman Al-Kababji, Faycal Bensaali, and Sarada Prasad Dakua. Scheduling techniques for liver segmentation: Reducelronplateau vs onecyclelr. In Akram Bennour, Tolga Ensari, Yousri Kessentini, and Sean Eom, editors, *Intelligent Systems and Pattern Recognition*, pages 204–212, Cham, 2022. Springer International Publishing.

[32] Hareem Kibriya, Momina Masood, Marriam Nawaz, and Tahira Nazir. Multiclass classification of brain tumors using a novel cnn architecture. *Multimedia Tools and Applications*, 81, 09 2022.

[33] Pragya Gupta, Jagannath Nirmal, and Ninad Mehendale. Custom cnn architectures for skin disease classification: binary and multi-class performance. *Multimedia Tools and Applications*, pages 1–28, 12 2024.

[34] Adnan Hussain, Muhammad Imad, Asma Khan, and Burhan Ullah. *Multi-class Classification for the Identification of COVID-19 in X-Ray Images Using Customized Efficient Neural Network*, pages 473–486. 01 2022.

[35] Shibani Santurkar, Dimitris Tsipras, Andrew Ilyas, and Aleksander Madry. How does batch normalization help optimization? In S. Bengio, H. Wallach, H. Larochelle, K. Grauman, N. Cesa-Bianchi, and R. Garnett, editors, *Advances in Neural Information Processing Systems*, volume 31. Curran Associates, Inc., 2018.

[36] Chaity Banerjee, Tathagata Mukherjee, and Eduardo Pasiliao. An empirical study on generalizations of the relu activation function. In *Proceedings of the 2019 ACM Southeast Conference*, ACMSE '19, page 164–167, New York, NY, USA, 2019. Association for Computing Machinery.

[37] Rahul Barman, Sharvari Deshpande, Shruti Agarwal, Unzela Inamdar, Manoj Devare, and Anita Patil. Transfer learning for small dataset. 03 2019.

[38] Nader Maray, Anne Hee Ngu, Jianyuan Ni, Minakshi Debnath, and Lu Wang. Transfer learning on small datasets for improved fall detection. *Sensors*, 23(3), 2023.

[39] Amsa Shabbir, Nouman Ali, Jameel Ahmed, Bushra Zafar, Aqsa Rasheed, Muhammad Sajid, Afzal Ahmed, and Saadat Hanif Dar. Satellite and scene image classification based on transfer learning and fine tuning of resnet50. *Mathematical Problems in Engineering*, 2021(1):5843816, 2021.

[40] Supriya Mahadevkar, Shruti Patil, Ketan Kotecha, and Ajith Abraham. A comparison of deep transfer learning backbone architecture techniques for printed text detection of different font styles from unstructured documents. *PeerJ Computer Science*, 10:e1769, 02 2024.

[41] Federica Gerace, Diego Doimo, Stefano Sarao Mannelli, Luca Saglietti, and Alessandro Laio. Optimal transfer protocol by incremental layer defrosting, 2023.